Investigation of the $^{12}C(\vec{p},d\pi^+)^{11}B$ reaction in the quasifree region

M. Benjamintz,* W. R. Falk, J. R. Campbell, and A. Green†
Department of Physics, University of Manitoba, Winnipeg, Manitoba, Canada R3T 2N2

P. G. Roos
Department of Physics and Astronomy, University of Maryland, College Park, Maryland 20742

P. L. Walden, S. Yen, and A. G. Ling‡
TRIUMF, 4004 Wesbrook Mall, Vancouver, British Columbia, Canada V6T 2A3

E. G. Auld
Department of Physics, University of British Columbia, Vancouver, British Columbia, Canada V6T 2A6

E. Korkmaz
Department of Physics, University of Northern British Columbia, Prince George, British Columbia, Canada V2N 4Z9

M. A. Punyasena§
Department of Physics, University of Alberta, Edmonton, Alberta, Canada T6G 2N5
(Received 10 July 1997; revised manuscript received 15 April 1998)

$^{12}C(\vec{p},d\pi^+)^{11}B$ has been investigated in the quasifree region at energies of 370 and 500 MeV. For each energy, measurements were made at the four angle combinations of $(\theta_{d,\mathrm{left}},\theta_{\pi,\mathrm{right}})$ equal to (15°, 30°), (15°, 55°), (25°, 30°), and (25°, 55°). In addition to strong excitation of the g.s. $3/2^-$ state, the 2.12 MeV $1/2^-$ and 5.02 MeV $3/2^-$ states are also excited with appreciable strength. Furthermore, a broad continuum at an excitation energy of about 20 MeV, corresponding to the $1s_{1/2}$ hole state is prominently seen. The pion differential cross section distributions exhibit maxima when the recoil nucleus momenta are at a minimum. Analyzing powers were obtained over the range of pion energies investigated. Several measurements for the $^2H(\vec{p},d\pi^+)n$ reaction are also reported. The results are compared with plane-wave impulse approximation and distorted-wave impulse approximation calculations. [S0556-2813(98)04808-0]

PACS number(s): 25.40.Qa, 21.45.+v, 24.70.+s

I. INTRODUCTION

Our present knowledge of the exclusive $^ZA(\vec{p},\pi^+)^Z(A+1)$ pion production reaction provides compelling evidence of the dominant role played by the underlying $pp\rightarrow d\pi^+$ reaction. The experimental evidence comes from a number of different investigations and comprises (i) the behavior of the analyzing powers in the $^ZA(\vec{p},\pi^+)^Z(A+1)$ reaction for discrete final states [1–3], and in the continuum [4] at excitation energies of about 20 MeV, (ii) the energy dependence of the $(\vec{p},\pi^+)$ differential cross section at fixed momentum transfer on a range of nuclei [5,6], and (iii) in the behavior of the differential cross section and analyzing powers of the $^{12}C(p,\pi^+)X$ reaction [7] in the quasifree region. Furthermore, the success of a phenomenological $pp\rightarrow d\pi^+$ model [8] applied in a detailed study of the $(\vec{p},\pi^+)$ reaction on ^2H, ^3He, ^4He, and ^{12}C provides much additional weight to this interpretation. Nevertheless, there remain many unanswered problems in $^ZA(\vec{p},\pi^+)^Z(A+1)$ reactions as to the interplay between the underlying reaction mechanism, complicated nuclear structure effects, the role of distortions, and other medium effects.

A number of these problems can be investigated by a kinematically complete measurement of the $^ZA(\vec{p},d\pi^+)^{Z-1}(A-1)$ reaction. In the $pp\rightarrow d\pi^+$ model of the $^ZA(\vec{p},\pi^+)^Z(A+1)$ reaction the latter is pictured as proceding via the primary $pp\rightarrow d\pi^+$ mechanism, followed by the capture of the deuteron in the nucleus $^{Z-1}(A-1)$ to form the final nucleus $^Z(A+1)$. Two momentum quantities are important in this picture, namely the momentum of the struck proton in the target and the momentum of the deuteron in the final nucleus. The values of these structure-dependent quantities can, to some degree, be selected by the kinematical variables chosen for the experiment, as shown in Fig. 4 of Ref. [8]. For the $^ZA(\vec{p},d\pi^+)^{Z-1}(A-1)$ reaction the same struck-nucleon momentum is important. In the limit of no distortions the struck-nucleon momentum and the recoil nucleus momentum have the same magnitudes. Thus the recoil nucleus momentum serves as an important kinematical variable. The range of kinematical variables readily acces-

*Present address: 304-5166 Halifax Street, Burnaby, B.C., Canada V5B 2N6.
†Present address: Physics Department, University of the Western Cape, Priv. Bag X17, Bellville 7535, South Africa.
‡Present address: RADEX, 3 Preston Ct., Bedford, MA 01730.
§Present address: Department of Physics, University of Kelaniya, Kelaniya, Sri Lanka.

TABLE I. Angle pairs (θ_d,θ_π) for the $(p,d\pi^+)$ measurements.

	Angle Combination			
	(15°,30°)	(15°,55°)	(25°,30°)	(25°,55°)
500 MeV	(15.5°,30.4°)	(15.6°,55.0°)	(24.9°,30.0°)	(25.0°,55.0°)
370 MeV	(15.5°,30.3°)	(15.6°,55.1°)	(25.0°,30.2°)	(25.0°,55.1°)

sible to experiment in the $^ZA(\vec{p},d\pi^+)^{Z-1}(A-1)$ reaction makes it possible to probe much of the dynamics of interest in the $^ZA(\vec{p},\pi^+)^Z(A+1)$ reaction. Pion absorption varies dramatically over this range, corresponding to mean free paths in nuclear matter from less than 1 fm to more than 5 fm. Interpretation of these results requires model calculations, which can be made via the distorted-wave impulse approximation (DWIA), for example.

The present study reports on measurements of the differential cross sections and analyzing powers for the $^{12}C(\vec{p},d\pi^+)^{11}B$ reaction carried out at proton energies of 370 and 500 MeV at the TRIUMF laboratory. No previous measurements of this reaction have been reported in the literature in this energy range; a single-angle measurement at 233 MeV has been reported [9]. In order to achieve the energy resolution necessary for resolving final nuclear states of interest the dual arm spectrometer system (DASS) was used, comprising the medium resolution spectrometer (MRS) and the second arm spectrometer (SASP). For each energy measurements were made at the four (nominal) angle combinations of (θ_d,θ_π) equal to (15°, 30°), (15°, 55°), (25°, 30°), and (25°, 55°). These angles are on the (left,right) side of the beam direction, respectively. Angle values pertaining to the actual measurements are given in Table I. The angles $\theta_d=15°$ and $\theta_d=25°$ correspond, roughly, to recoil nucleus momenta in the range ($\geqslant$100 MeV/c) and ($\geqslant$200 MeV/c), respectively. This situation applies if, in a plot of p_d vs p_π, the ''upper'' kinematic locus is selected, as was the case in the present experiment. The ''lower'' locus corresponds to much higher recoil-nucleus momenta (typically $\geqslant$300 MeV/c, and correspondingly much lower probabilities for observing these momenta). For ^{12}C the $1p$-shell momentum distribution has a broad peak in the neighborhood of $\approx$100 MeV/c. A momentum of 200 MeV/c is in the tail of this distribution but is still quite probable in the ^{12}C nucleus. These are roughly the two regimes investigated in this experiment.

The smallest deuteron angle of $\theta_d=15°$ is, of course, larger than the maximum angle in the free $pp\rightarrow d\pi^+$ reaction. This limitation was imposed by the physical constraints of the spectrometers. However, because the binding energy of the p-shell proton in ^{12}C the free $pp\rightarrow d\pi^+$ reaction kinematics can not be obtained in any case. Indeed, for all the angle pairs under study the recoil nucleus carries off only a few MeV of energy at most; hence the sum of the pion and deuteron energies is approximately constant at 345 MeV (for 500 MeV bombarding energy), some 16 MeV lower than in the free $pp\rightarrow d\pi^+$ reaction. Furthermore, since the p-shell momentum wave function in ^{12}C is a maximum at $\approx$100 MeV/c, kinematics that select approximately 100 MeV/c for the recoil nucleus momentum will result in a large cross section. This choice minimizes the dependence upon distortions to bring about the required momentum sharing, and thus approximates the quasifree condition. By the same token, selecting a recoil nucleus momentum of $\approx$0 MeV/c will result in a very small cross section. Such a choice necessarily emphasizes distortion effects. The kinematics selected in the present study do not place the reaction very far off shell. Indeed, relative to those conditions under which the $(p,2p)$ reaction and similar reactions have been studied, off-shell effects should not be very large.

The laboratory pion angle effectively selects the center of mass (c.m.) angle at which the underlying $pp\rightarrow d\pi^+$ process occurs in the $^ZA(\vec{p},d\pi^+)^{Z-1}(A-1)$ reaction. In the approximate c.m. frame of the incident and struck proton the pion is produced at c.m. angles of 48°, 82°, 42°, and 74°, at the four angle combinations given above, respectively. These c.m. angles depend on the selected kinematics and are specified for 500 MeV at the minimum value of the recoil nucleus momentum (where the cross section is a maximum). Since the $pp\rightarrow d\pi^+$ reaction exhibits a strong angular dependence of the differential cross section and the analyzing power these two pion angles of 30° and 55° select two quite different regimes for this reaction. A limited number of measurements were also made for the $^2H(\vec{p},d\pi^+)n$ reaction.

II. EXPERIMENT

A. Polarized proton beam

The experiment was performed in the proton hall of the TRIUMF laboratory by using two magnetic spectrometers, as noted above. Polarized proton beams from the optically pumped ion source were extracted from the TRIUMF cyclotron at energies of 500 MeV (with -6 cm/% dispersion) and 370 MeV (achromatic). Beam intensities ranged from 5 to 30 nA, depending on spectrometer angles, and the beam polarization was typically 65%. A natural carbon target and a CD_2 target of areal densities 50.2 mg/cm^2 and 200 mg/cm^2, respectively, were used.

The number of beam protons N_p was measured by using an in-beam polarimeter (IBP) [10] and a secondary emission monitor (SEM) [10,11], positioned upstream and downstream of the target, respectively. These two instruments were calibrated in previous experiments by using a Faraday cup and provided independent measurements of the beam intensity which agreed to within 5%. Beam polarization P was measured by using the IBP.

B. Spectrometers

Deuterons from the $^ZA(\vec{p},d\pi^+)^{Z-1}(A-1)$reaction were detected in the MRS spectrometer [12]. The MRS is a vertical bend quadrupole-dipole (QD) 1.6 GeV/c spectrometer with a momentum acceptance $\Delta p/p$ of $\pm$6%. It is instru-

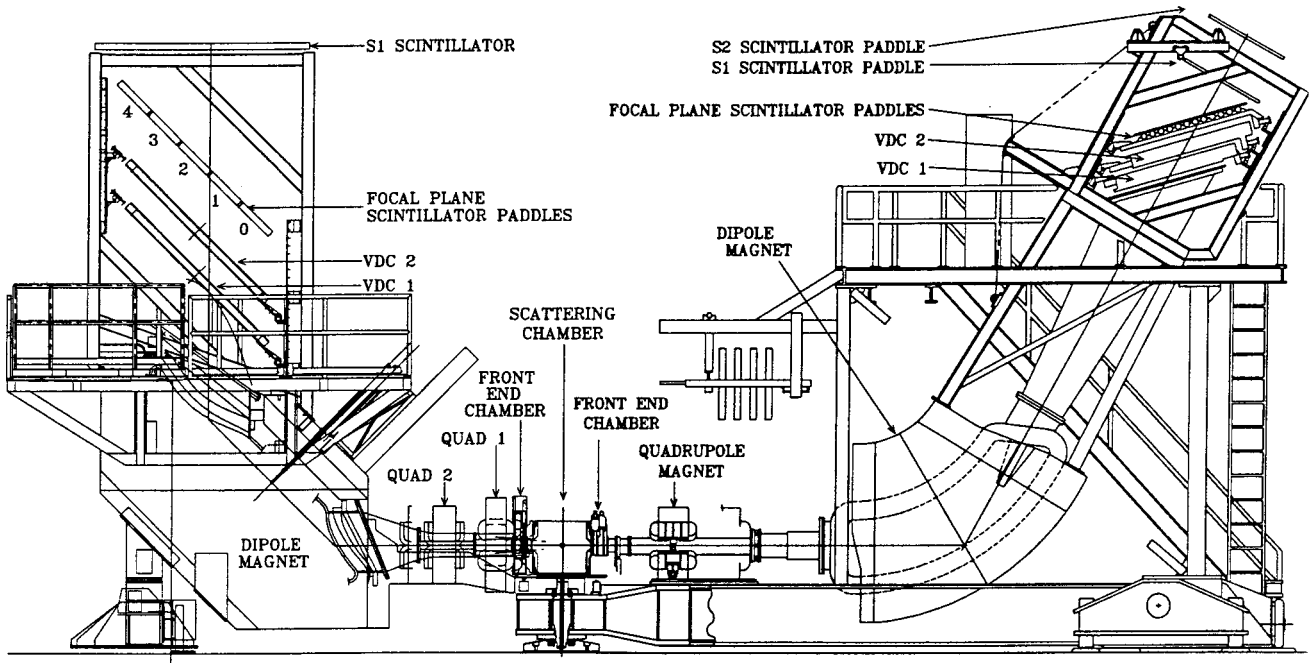

FIG. 1. Schematic of the spectrometers SASP (left) and MRS (right). The front end chamber is located just outside the scattering chamber for each spectrometer. The focal plane vertical drift chambers are designated VDC1 and VDC2.

mented with a front end multiwire drift chamber (FEC) at the entrance to the quadrupole, and two vertical drift chambers (VDC) and a scintillator hodoscope at the exit of the dipole. Good track reconstruction is provided by the chamber information, and particle identification from particle time of flight and energy loss in the scintillator hodoscope. An absolute momentum calibration of the MRS was performed by using data from the $^{12}C(p,p')^{12}C$ reaction to the g.s., 4.44 MeV, and 9.64 MeV states, at 280 MeV proton bombarding energy. These data were also used in mapping the acceptance of the spectrometer. The above calibration required an independent measurement of the absolute cyclotron energy, which was determined from a comparison of detected particle momenta of protons from pp scattering and pions from the $pp \rightarrow d\pi^+$ reaction. A schematic of the MRS spectrometer, as well as the SASP spectrometer discussed below, is shown in Fig. 1.

Pions were detected in the SASP spectrometer [13]. This spectrometer is a quadrupole-quadrupole-dipole (QQD) magnetic system and has a solid angle of about 12 msr and a momentum acceptance $\Delta p/p$ extending beyond -10 and $+15$ %. Because of the shorter flight path of 7 m it is more suited for pion detection than the MRS. The resolution at the design central momentum of 660 MeV/c is 0.02% $\Delta p/p$. A more detailed account of the design and operating parameters of the spectrometer will be presented [14]. As with the MRS, it is instrumented with a front end multiwire drift chamber at the entrance to the first quadrupole, and two vertical drift chambers and a scintillator hodoscope at the exit of the dipole. In the present experiment it was found that a very clean $d-\pi$ coincidence signal could be obtained without the use of the SASP FEC. By removing this FEC from the event trigger considerably higher beam currents could be tolerated. Particle identification of the pions was obtained from particle time of flight (with respect to the cyclotron rf) and energy loss in the scintillator.

A consequence of the large acceptance of SASP is that particles detected in the focal plane have traversed distances from the target which vary substantially. In order to make appropriate corrections for the decay of pions a comprehensive Monte Carlo study was undertaken. Particle rays from a uniform distribution over the angular acceptance of the spectrometer and with a momentum distribution $\Delta p/p$ from -15 to $+20$% at the target were traced through the system. The subsequent history of each event, for which the position, angles, and path length were known at the focal plane, was followed through the VDC's and the scintillator hodoscope. Muons from pions which decay inside the dipole, and before reaching the VDC's, are presumed lost to the detector system; those from pions decaying after the second VDC are often detected in the hodoscope and appear as valid events. The laboratory distribution of the muon events about the initial pion direction was treated in detail in calculating the intersection of such events in the detectors of the hodoscope. The resulting effective length of the spectrometer for pions depends on the central momentum setting and the location of the event on the focal plane. A convenient way of expressing the latter is via the percentage momentum deviation from the central momentum $\delta=(p-p_0)\times 100/p_0$, where p is the momentum of the particle and p_0 is the central momentum. The central momentum (in units of MeV/c) is related to the magnetic field setting by the equation $p_0=50.311\times B_s$, where B_s is the SASP dipole field in kG at the ''$x=15$ in.'' reference point. These Monte Carlo results were parametrized to produce an effective length $L_{\rm eff}=f(\delta,p_0)$, from which the pion survival probability η_π was calculated by using the expression $\eta_\pi=\exp[(-139.57\times L_{\rm eff})/(\tau c\times p)]$. Here $\tau c=780.45$ cm, is the pion decay length, $L_{\rm eff}$ is the effective length in cm, and p is the pion momentum in MeV/c.

The solid angle of SASP at $p=p_0$ was calibrated by using the known cross section [15,16] for the $pp \rightarrow d\pi^+$ reaction at

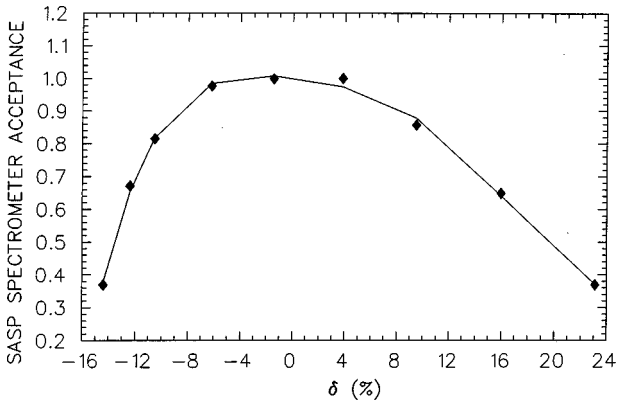

FIG. 2. SASP spectrometer relative solid angle acceptance as a function of δ.

500 MeV. This, together with the pion decay correction yielded a central solid angle of 12 msr. Likewise, this reaction and the pion decay correction were used to map the SASP solid angle acceptance as a function of δ. The relative solid angle acceptance ϵ_{SASP} normalized to unity at the central momentum, is shown in Fig. 2, where the points are the experimental measurements and the solid line is the fitted curve. This acceptance remains at significant values beyond the nominal design limits of -10 and $+15\%$. Typically, four or five pairs of momentum settings of the two spectrometers were required at each angle pair in order to map out the particle momentum distributions over the desired range for the $^{Z}A(\vec{p},d\pi^+)^{Z-1}(A-1)$ reaction.

III. ANALYSIS

A master trigger was generated from coincidence events, loosely defined as a deuteron in the MRS in coincidence with a pion in SASP. In the separate spectrometer arms a deuteron event required a signal in one of the planes of the MRS FEC (timing signal) and a signal in the first plane of VDC1, together with appropriate energy loss in the scintillator hodoscope. In addition, a signal in a scintillator $S1$ positioned beyond the hodoscope. was also required. The pion event required a signal in the first plane of the SASP VDC1, and appropriate energy loss in the scintillator hodoscope. The trigger was subsequently inhibited while all the electronics were read out and recorded by the computer. Computer system livetime η_{comp} was obtained from the ratio of the number of recorded events to the number of master triggers. Typically, this livetime was well above 90%, occasionally dropping to 80% for some of the higher rate settings. Online and offline analysis of the data was carried out by using the data analysis program NOVA [17].

Composite wire chamber efficiencies were defined for the chambers in each of the MRS and SASP as follows: $\eta_{\mathrm{MRS}}=N_{\mathrm{FEC\ VDC1\ VDC2}}/N_{\mathrm{deuterons}}$, $\eta_{\mathrm{SASP}}=N_{\mathrm{VDC1\ VDC2}}/N_{\mathrm{pions}}$, where $N_{\mathrm{FEC\ VDC1\ VDC2}}$ is the number of events where each of the chambers has one, and only one, properly decoded track, and $N_{\mathrm{deuterons}}$ is the total number of deuteron events. For pions the quantities $N_{\mathrm{VDC1\ VDC2}}$ and N_{pions}, are similarly defined. At first sight these definitions would appear to result in incorrectly high values for the efficiencies, since the very definitions of $N_{\mathrm{deuterons}}$ and N_{pions}, require signals in selected chambers, as described. However, extensive intercomparisons with one-, two-, and all-plane efficiencies showed that the former provided a good estimate of the chamber efficiencies. Apparently, even when a wire chamber plane does not decode as a good event, it generally produces a signal sufficient to satisfy all the timing requirements. Typically η_{MRS} was found to be between 50 and 55 % and η_{SASP} about 80%. The lower value for η_{MRS} was due primarily to the high singles rate in the FEC, which resulted in undecodable multiple tracks.

TABLE II. Angular acceptance at spectrometer entrance.

	Nonbend plane half angle (mr)	Bend plane half angle (mr)
MRS(d)	19.7	31.8
SASP(π)	34.5	86.6

By using the information from the wire chamber coordinates the deuteron and pion trajectories were reconstructed. Tracks which did not reconstruct as originating from the target were rejected.

The solid angle of the MRS spectrometer was determined by software cuts applied to the FEC. A series of such cuts were applied, defining solid angles from much less to greater than the known acceptance. The resulting yields of deuteron events extrapolated linearly to a solid angle of 2.5 msr. Reconstructed angles at the target for pion events in the SASP spectrometer were not known with sufficient accuracy to use these for defining the solid angle. However, again with a series of different angle cuts, it was ascertained that the angle cuts actually employed in the cross section calculations encompassed a full acceptance of the spectrometer of 12 msr, as previously discussed. The angular acceptances at the entrances to the spectrometers are given in Table II.

The offline analysis of the data revealed that there were normalization problems with the first measurements taken during the course of the experiment. The affected data were those measurements taken at 500 MeV for both the ^{2}H and ^{12}C targets at the angle combinations (15°,30°) and (15°,55°). After careful reexamination of all the scaler data and the software analysis it seemed most unlikely that these problems were related to beam normalization, chamber efficiency problems, etc., all of which exhibited normal patterns. More likely, the problem was of an electronic nature involving coincidence inefficiency between the two spectrometers. There was no suggestion in any of the results that there was a spin dependence associated with this normalization problem. Consequently, the analyzing power results for these angle pairs are believed not to be compromised.

IV. RESULTS

A typical plot of deuteron momentum vs pion momentum for the $^{12}C(\vec{p},d\pi^+)^{11}B$ reaction is shown in Fig. 3. The most prominent band corresponds to the ^{11}B g.s., and the two other discernable bands to the 2.12 MeV $1/2^-$ and 5.02 MeV $3/2^-$ excited states. Events below the bands arise from excitation of the broad $1s_{1/2}$ hole state, centered at about 20 MeV excitation. A measure of the random coincidence rate is given by the density of events in the region above the bands.

From the measured momenta and the reconstructed trajec-

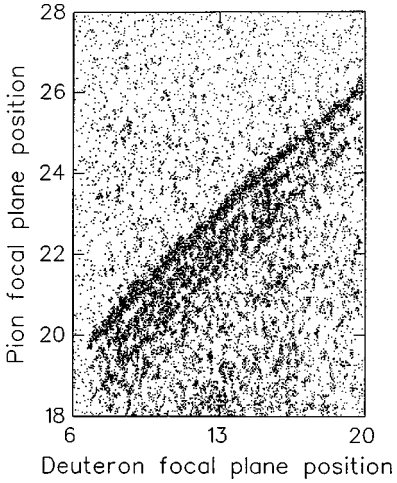

FIG. 3. Pion-deuteron coincidence events from the $^{12}C(\vec{p},d\pi^+)^{11}B$ reaction at 500 MeV for $\theta_d = 15.5°$ and $\theta_\pi = 30.4°$. The deuteron momentum increases to the left and the pion momentum increases in the upwards direction. The g.s. locus spans a deuteron momentum interval of 80 MeV/c at a central momentum of 653 MeV/*c*; the corresponding pion momentum interval is 27 MeV/*c* at a central momentum of 337 MeV/*c*. The focal plane positions are in arbitrary units.

tories the missing mass for each event was calculated. Figure 4 shows a typical result of such a missing mass plot, where the ^{11}B g.s. rest mass has been subtracted to yield the excitation energy. The panels show the total spin-up and spin-down events; a nonzero analyzing power is clearly indicated. Random coincidence events have been subtracted from these plots. Although some contribution from other states close to the 2.12 and 5.02 MeV states cannot be ruled out, it is expected that this will be small, judging from the observations

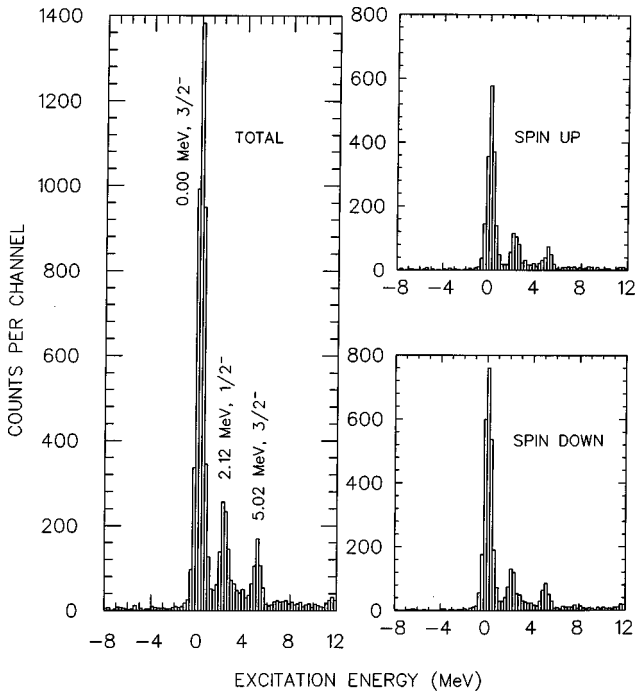

FIG. 4. Excitation energy plot for the $^{12}C(\vec{p},d\pi^+)^{11}B$ at 500 MeV for $\theta_d = 15.5°$ and $\theta_\pi = 30.4°$.

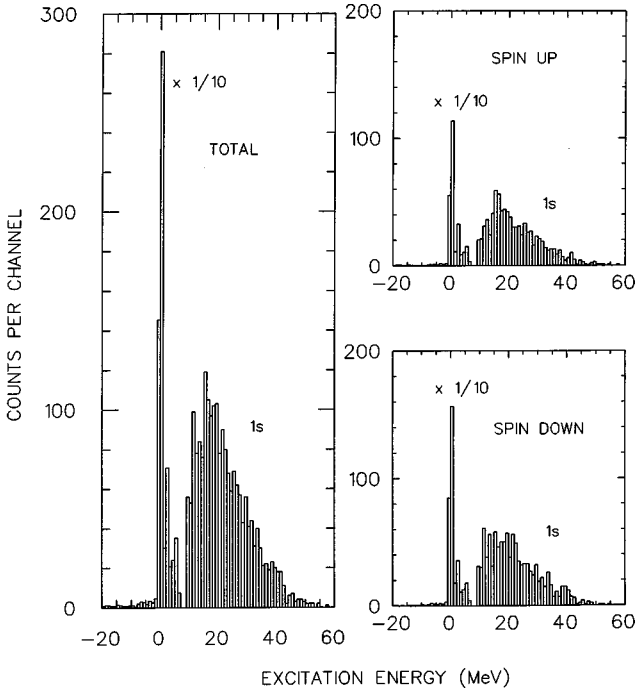

FIG. 5. Excitation energy plot of Fig. 4 extended to 60 MeV. The low excitation region has been supressed by a factor of 10. The broad distribution arises from the 1*s* hole state.

in proton pickup reactions [18]. The missing mass resolution in this figure is about 750 keV, most of which arises from the energy loss spread of the deuterons in the target.

Optical aberration corrections in the SASP spectrometer are large, particularly those involving the θ coordinate, the bend-plane scattering angle (as defined in TRANSPORT [19]). These aberrations were corrected in software replay of the data. At the time of this analysis a complete set of these aberration corrections had not been compiled and empirical corrections involving this coordinate were applied. As well, the momentum calibration for SASP, carried out for 660 MeV/*c* protons, was found to be inappropriate for the much lower momentum pions. Empirical corrections to the momentum calibration were deduced from an initial analysis pass through the data.

Figure 5 shows the missing mass plot of Fig. 4 extended to 60 MeV excitation energy in ^{11}B. Although the spectrometer acceptances record only some unknown fraction of the latter events, strong excitation of the broad $1s_{1/2}$ hole state is indicated. The absolute cross section for this state is very difficult to determine. Not only does it depend on the convolution of the spectrometer acceptances near the edges of one or both of the spectrometers, it also depends on model predictions of the strength distribution of this state as a function of excitation energy. For this reason we choose to speak only of a measured lower limit for the cross section for this state.

Analyzed events were stored in a two-dimensional (2D) array of δ_s (the SASP percentage momentum deviation) vs missing mass for subsequent calculations of the differential cross sections and analyzing powers. In order to adequately account for the large variations in ϵ_{MRS}, ϵ_{SASP}, and η_π associated with different events, the quantity $1/(\epsilon_{\mathrm{MRS}}\,\epsilon_{\mathrm{SASP}}\,\eta_\pi)$, was stored for each event in a 2D array of

the same dimensions as above. This latter array thus contains the yield information normalized for the relative spectrometer acceptances and the pion survival fraction. For each state of interest the range of δ_s was further binned into 2–5 intervals, $\Delta_{\delta s}$ depending on the number of events available. These latter intervals are thus intervals in p_π.

The cross section for a given interval was calculated according to the expression

$$d^3\sigma/d\Omega_d d\Omega_\pi dp_\pi = [N_{\pi d}/(\bar{\epsilon}_{\rm MRS}\cdot\bar{\epsilon}_{\rm SASP}\cdot\bar{\eta}_\pi)]/[N_p N_t \eta_{\rm comp}\eta_{\rm MRS}\eta_{\rm SASP}\Delta\Omega_d\Delta\Omega_\pi\Delta p_\pi)].$$

Here $N_{\pi d}$ is the number of events, $\bar{\eta}_\pi$ the average pion survival fraction and $\bar{\epsilon}_{\rm MRS}$ and $\bar{\epsilon}_{\rm SASP}$ the average relative focal plane acceptances of the MRS and SASP, respectively, all within the given interval. These quantities were all obtained from the two 2D arrays as explained. N_p and N_t are the number of incident protons and the number of target nuclei per cm^2, respectively, and $\eta_{\rm comp}$ is the data acquisition computer livetime. Spectrometer solid angles are given by $\Delta\Omega_d$ (MRS) and $\Delta\Omega_\pi$ (SASP). The pion momentum interval is Δp_π. This expression applies to the total, spin up or spin down cross section, depending on the selected input quantities.

Denoting the differential cross section of the above expression simply by σ, for brevity, the spin averaged differential cross section is given by

$$\sigma = [P(\downarrow)\sigma(\uparrow) + P(\uparrow)\sigma(\downarrow)]/[P(\uparrow)+P(\downarrow)].$$

Here $\uparrow$ and $\downarrow$ refer to the spin up and spin down direction of the incident beam polarization, respectively. The analyzing power is given by the expression

$$A_{N0} = [\sigma(\uparrow)-\sigma(\downarrow)]/[P(\downarrow)\sigma(\uparrow)+P(\uparrow)\sigma(\downarrow)].$$

Experimental results of the differential cross sections and analyzing powers as a function of the pion momentum are shown in Fig. 6 for the $^2H(\vec{p},d\pi^+)n$ reaction. Measurements were made at two angle pairs for each of the two energies. These measurements were possible over a limited kinematic range only, by using a CD_2 target, because of interference from the $^{12}C(\vec{p},d\pi^+)^{11}B$ reaction. Figures 7 and 9 show the results for the $^{12}C(\vec{p},d\pi^+)^{11}B$ g.s. reaction at 500 and 370 MeV, respectively. All quantities shown in Figures 6–14 are evaluated in the laboratory frame. The errors shown represent the statistical uncertainties; the overall normalization uncertainty in the cross sections is $\pm 15\%$, except for those cases noted at the end of the previous section where normalization problems were experienced. Theoretical curves shown in the above figures will be discussed in the next section. Results for the excited states are shown in Figs. 11–14.

The cross section distributions as a function of pion momentum shown in the above figures are roughly Gaussian in shape and have typical widths of 100 MeV/c for the $^{12}C(\vec{p},d\pi^+)^{11}B$ reaction and about 50 MeV/c for the $^2H(\vec{p},d\pi^+)n$ reaction. Peak cross sections for the former reaction are in the range of 2–6 μb/(sr^2 MeV/c) at 500 MeV and 1–3 μb/(sr^2 MeV/c) at 370 MeV. The recoil nucleus momentum p_R is also indicated in each of the cross section plots referred to above. The peak in the cross section distribution occurs at a pion momentum which corresponds closely to the minimum in the value of p_R.

Over the range of the measurements the analyzing powers exhibit a fairly gentle variation with pion momentum, with values predominantly in the positive (0.0 to 0.4) range for 500 MeV, and values predominantly in the negative (0.0 to -0.3) range for 370 MeV, for the $^{12}C(\vec{p},d\pi^+)^{11}B$ g.s. reaction.

V. THEORY

A. DWIA and PWIA calculations

The experimental results are interpreted in terms of a factorized amplitude distorted-wave impulse approximation (DWIA) theory [20,21]. The calculations were carried out by using the code THREEDEE [22], an earlier version of which was applied to this same reaction at 223 MeV [9]. The underlying physics assumption in these calculations is that the pion production in the three-body $^ZA(\vec{p},d\pi^+)^{Z-1}(A-1)$ reaction is mediated by the two-body $pp\rightarrow d\pi^+$ process. Thus we assume that the incoming proton interacts with a bound proton in the nucleus leading to a final state deuteron and pion, and leaving the residual nucleus in a single hole state. We briefly outline the DWIA formulation in the following.

Although THREEDEE can treat nuclei of arbitrary angular momentum, for clarity in the expressions presented here, we consider the case of a spin zero target. Therefore in our DWIA model the reaction proceeds with the removal of a nucleon of unique orbital and total angular momentum leading to a hole state in residual nucleus B with the angular momentum of the struck particle. We write the cross section for this $^ZA(\vec{p},d\pi^+)^{Z-1}(A-1)$ reaction induced by a polarized proton with polarization ρ_a incident on the nucleus A with total angular momentum $J_A=0$ and leading to a final nuclear state of angular momentum j as

$$\sigma_{BA}(\rho_a) = \frac{2\pi}{\hbar c}\omega_B\sqrt{A}\sum_{m\rho_d}\left|\sum_{\lambda\sigma\sigma'_a}\mathcal{I}_{AB}(nlsjt)\times(l\lambda s\sigma|jm)T^{l\lambda}_{\sigma'_a\rho_a}\langle\rho_d,\mathbf{k}'_\mathbf{d}\mathbf{k}'_\pi|\mathbf{t}|\sigma;\sigma'_\mathbf{a},\mathbf{k}_\mathbf{a}\rangle\right|^2, \quad (1)$$

where ω_B is the energy density of final states. For the struck nucleon the quantum number j (projection m), represents the total angular momentum which is composed of angular momentum l (projection λ) and spin $s=\frac{1}{2}$ (projection σ). The

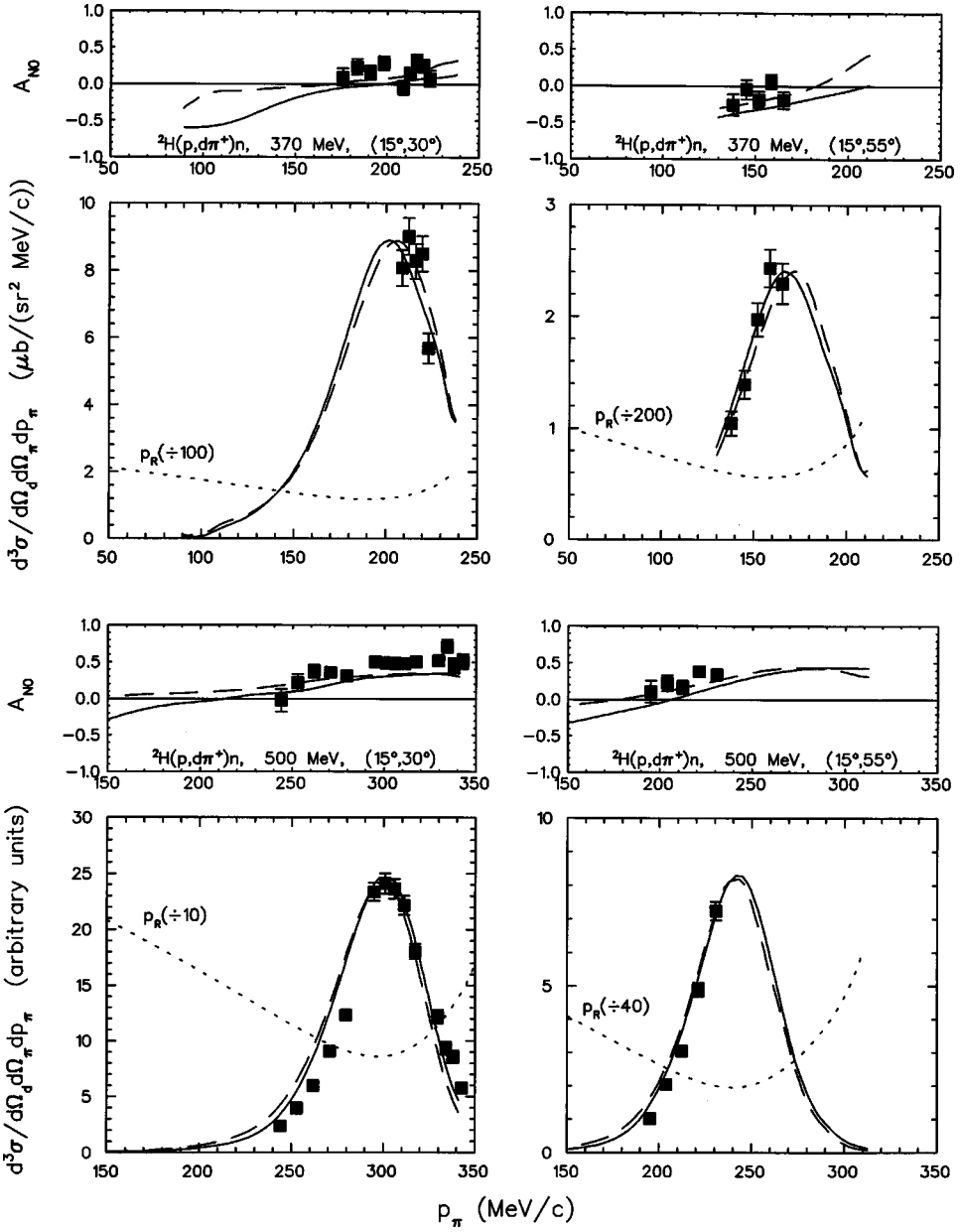

FIG. 6. Analyzing powers and differential cross sections for the $^2\mathrm{H}(\vec{p},d\pi^+)n$ reaction at 370 and 500 MeV. The curves are PWIA calculations RH1 (solid line), and RH2 (long dashes), as described in Table IV. The dotted curve represents the recoil momentum in units of MeV/c. All quantities are expressed in the laboratory frame. The cross section curves have been normalized to the data as shown.

quantity in brackets is the vector coupling coefficient. The spectroscopic amplitude $\mathcal{I}_{AB}$ is related to the conventional single nucleon spectroscopic factor through $C^2S=A\times\mathcal{I}_{AB}^2$, where A is the number of target nucleons. The matrix element $\langle\rho_d,\mathbf{k}_d';\mathbf{k}_\pi'|\mathbf{t}|\sigma;\sigma_a',\mathbf{k}_a\rangle$ is the two-body amplitude for the production of a pion by a proton (spin projection σ_a',) incident on a target proton (spin projection σ) leading to a deuteron (spin projection ρ_d) and a π^+. These amplitudes are assumed to be the on-shell amplitudes and are taken from the work of Ref. [16].

The effects of distortion are contained in

$$T^{l\lambda}_{\sigma_a'\rho_a}=\int \chi_d^{(-)*}(\mathbf{k_d'})\chi_\pi^{(-)*}(\mathbf{k_\pi'})\phi_{l\lambda}\chi^{(+)}_{\sigma_a'\rho_a}(\mathbf{k_a})d^3r, \quad (2)$$

where the $\chi^{(-)}$'s represent distorted waves for the emitted pion and deuteron and $\chi^{(+)}$ represents the incoming proton which can flip its spin due to the spin-orbit force in the optical potential. Note that in this formulation we have ignored the spin of the deuteron in the deuteron distorted wave, since THREEDEE does not incorporate a spin-orbit potential for spin one particles. Although analyzing powers are large in elastic deuteron scattering, we do not expect the neglect of the spin-orbit potential for the final state deuteron to have a large effect on an initial state spin observable such as the beam analyzing powers measured in the current experiment. Calculations of the spin transfer to the deuteron would of course be expected to show significant effects due to the deuteron spin-orbit potential, but these were not measured. The spatial part of the struck nucleon wave function is represented by $\phi_{l\lambda}$.

The unpolarized cross sections and analyzing powers are

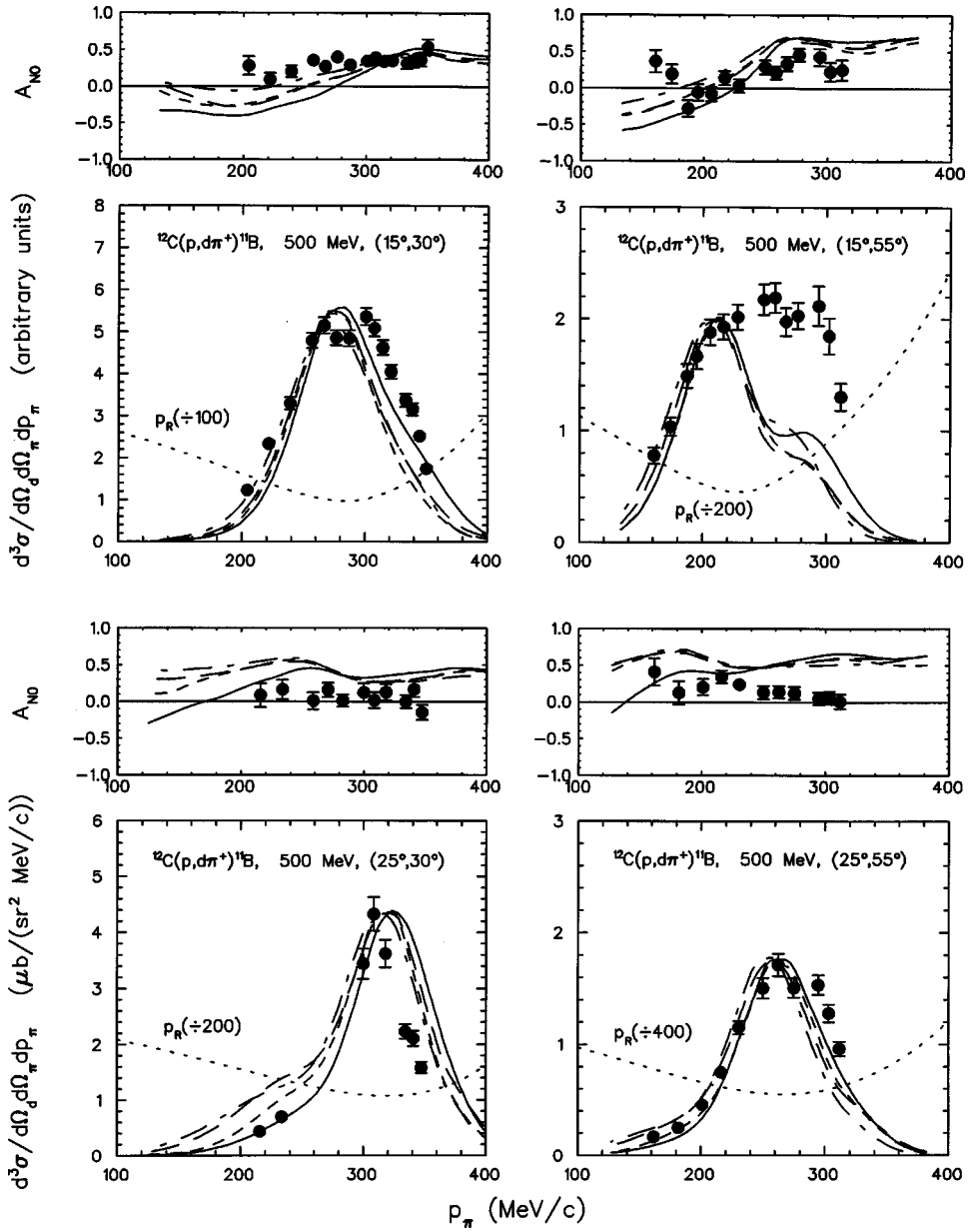

FIG. 7. Analyzing powers and differential cross sections for the $^{12}C(\vec{p},d\pi^+)^{11}B$ reaction at 500 MeV for the four angle pairs. The curves are DWIA calculations RC1 (solid line), RC2 (long dashes), RC3 (dash-dot curve), and RC4 (short dashes), as described in Table V. The dotted curve represents the recoil momentum in units of MeV/*c*. All quantities are expressed in the laboratory frame. The cross section curves have been normalized to the data as shown.

formed from the usual average and difference of the calculated cross sections for $\rho_a = \pm\frac{1}{2}$, respectively. As has been pointed out for other three-body reactions (e.g., $A(\gamma,\pi N)B$ [23] or $A(\pi,\pi N)B$ [24]), the analyzing powers calculated in the DWIA for the three-body reactions are closely related to the two-body spin observables, particularly the analyzing power for $s_{1/2}$ nucleon removal. For the present case, if one ignores the effects of the spin-orbit potential on the incident proton ($\sigma'_a = \rho_a$), we see from Eq. (1) that the $^{Z}A(\vec{p},d\pi^+)^{Z-1}(A-1)$ three-body analyzing power for $s_{1/2}$ removal is identical to the two-body $\vec{p}p \rightarrow d\pi^+$ analyzing power and unaffected by distortion effects. As we shall see in the next section, even with the addition of the incident proton spin-orbit potential, the $^{Z}A(\vec{p},d\pi^+)^{Z-1}(A-1)$ beam analyzing power is very similar to that of $\vec{p}p \rightarrow d\pi^+$.

The cases of $p_{3/2}$ and $p_{1/2}$ removal are somewhat more complicated, since in these cases distortions introduce an effective polarization of the bound nucleon. This has been noted for other reactions and is often referred to as the Newns effect [25] or Maris effect [26]. Given the fact that both the incoming and outgoing particles are strongly interacting and attenuated, we might expect the effective polarization in the present reaction to be rather large. Again in the DWIA, ignoring the effect of the spin-orbit potential on the incident proton and assuming a coplanar geometry for the three-body $^{Z}A(\vec{p},d\pi^+)^{Z-1}(A-1)$ reaction, a relatively simple expression can be derived relating the three-body beam analyzing powers for *p*-shell nucleon removal to the two-body $\vec{p}p \rightarrow d\pi^+$ analyzing powers (see, for example, Ref. [24]). To do so we introduce the effective polarization

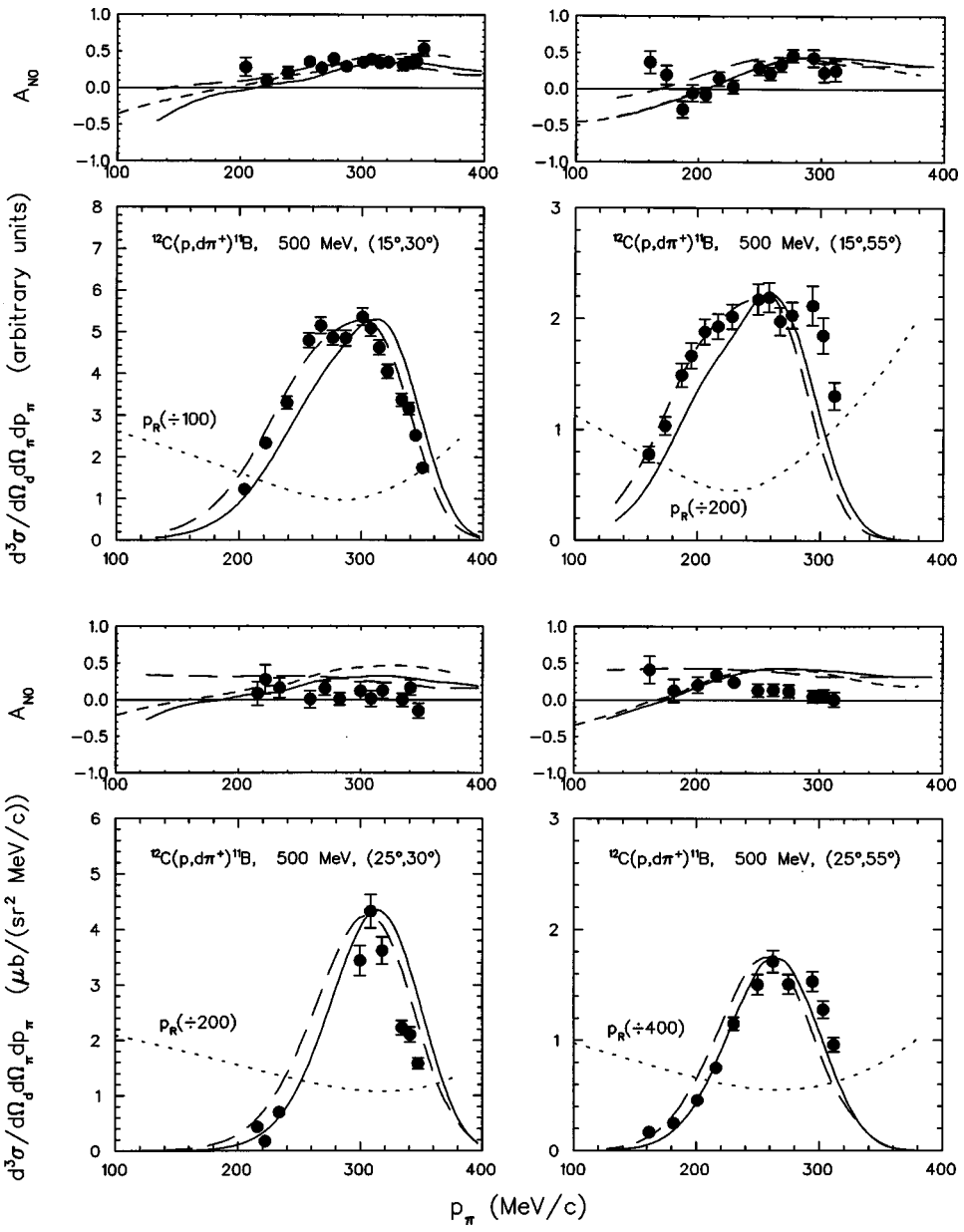

FIG. 8. The same as Fig. 7, with PWIA calculations RC5 (solid line), RC6 (long dashes), FC1 (short dashes, analyzing powers, only), as described in Table V.

in orbital angular momentum induced by the distortion effects as

$$P=\frac{|T^{11}|^2-|T^{1-1}|^2}{|T^{11}|^2+|T^{1-1}|^2}. \tag{3}$$

It is then possible to write a simplified expression for the cross section of an incoming proton with spin projection $\rho_a = \pm\frac{1}{2}$ on a spin zero target as

$$\sigma\left(\rho_a=\pm\frac{1}{2}\right)=\sigma_0^{3b}(1\pm A_{00n0}^{2b}+\alpha P A_{000n}^{2b}\pm\alpha P A_{00nn}^{2b}), \tag{4}$$

where σ_0^{3b} is the unpolarized cross section. The quantities A_{00n0}^{2b}, A_{000n}^{2b}, and A_{00nn}^{2b} are the beam analyzing power, the target analyzing power (equal to the beam analyzing power), and the spin correlation parameter for the two-body $\vec{p}p \rightarrow d\pi^+$ reaction, respectively. The quantity α relates the orbital polarization to a spin polarization and has the value of -1 for $p_{1/2}$ and $+\frac{1}{2}$ for $p_{3/2}$. Clearly the three-body beam analyzing power will directly depend on the two-body analyzing power, but in addition the two-body spin correlations will play a significant role.

As with all DWIA calculations various choices of phenomenological input are required. In our calculations single particle bound-state wave functions for the struck proton in ^{12}C were generated with the Woods-Saxon potential parameters of Elton and Swift [27]. For ^{2}H, the wave function was obtained from the Paris potential, and included both $L=0$ and $L=2$ components. The incoming proton distorted waves were generated by using a Schrödinger equivalent reduction of the global Dirac-equation based optical model analysis of Cooper *et al.* [28]. For the emitted deuteron two different optical model potentials were employed. The first was ob-

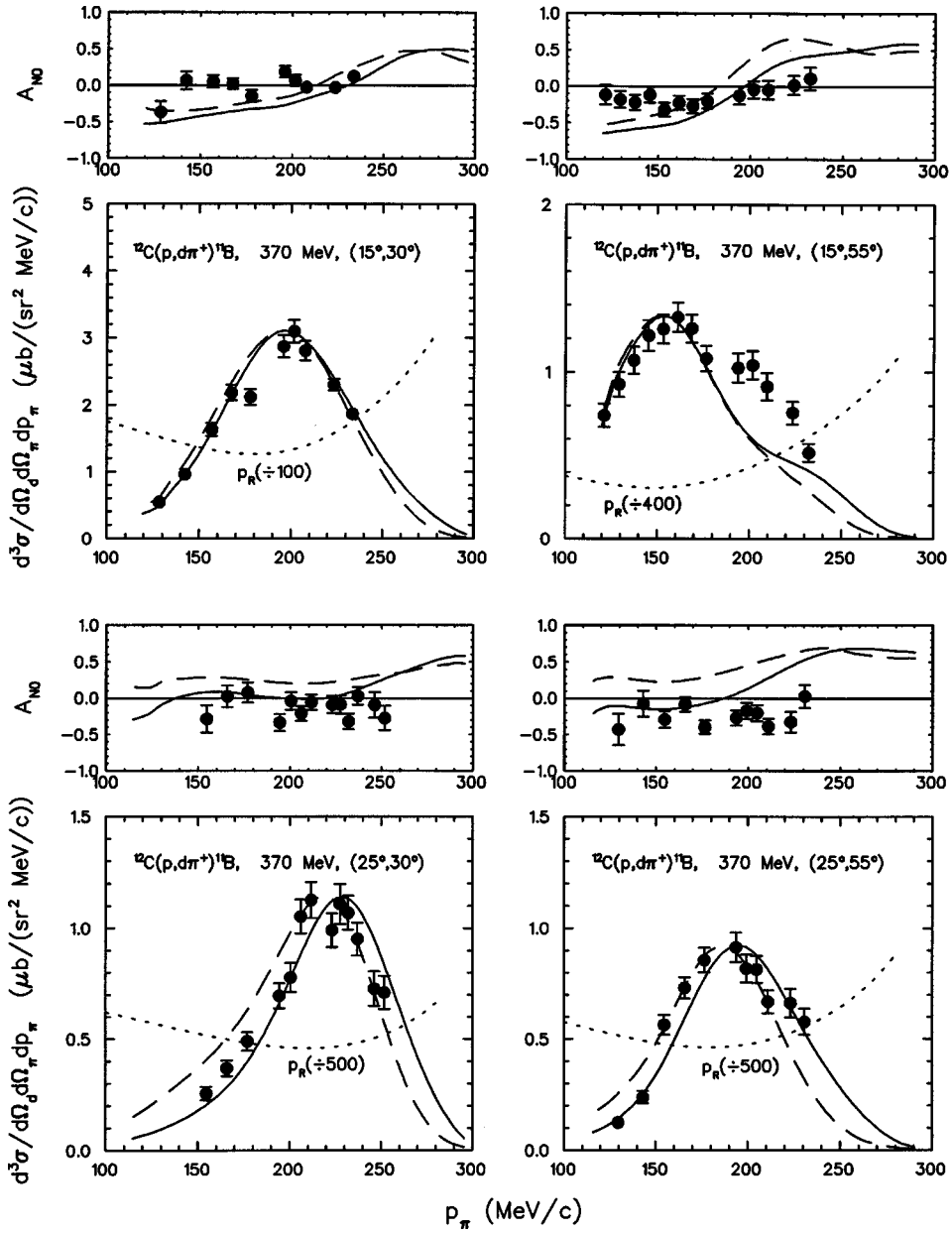

FIG. 9. Analyzing powers and differential cross sections for the $^{12}C(\vec{p},d\pi^+)^{11}B$ reaction at 370 MeV for the four angle pairs. The curves are DWIA calculations RC1 (solid line), and RC2 (long dashes), as described in Table VI. The dotted curve represents the recoil momentum in units of MeV/*c*. All quantities are expressed in the laboratory frame. The cross section curves have been normalized to the data as shown.

tained by simply doubling the Nadasen-Schwandt [29] proton potential at half the deuteron energy, i.e., at the same kinetic energy per nucleon. The second was obtained from an extrapolation of the parameters for $d+^{12}C$ scattering from Bojowald *et al.* [30]. Although these potentials are energy dependent, DWIA calculations revealed that the differences between the results assuming an energy-dependent and an energy-independent potential were quite small. Indeed, they were no greater than the differences between the results for the two different potentials described above. Hence, because of the greater convenience, energy-independent forms of the potentials were used. These potentials, both of a Woods-Saxon form, will be referred to as V_{d1} and V_{d2}, respectively. Details of the parameters for these potentials are given in Table III.

Pion distorted waves were generated from two different potentials as well, both of the Kisslinger type. The work of Cottingame and Holtkamp [31] was used for the first. These potentials use the Kisslinger form with potential strengths b_0 and b_1 obtained from the pion-nucleon *t* matrix, but shifted in energy by about 28 MeV. The density was taken to have a modified harmonic oscillator form, with parameters $a=1.60$ and $\alpha=1.01$. This potential is thus energy dependent. The other potential was obtained from a fit to $\pi+^{16}O$ elastic scattering at 163 MeV. The density, taken to have a Fermi form, used parameters $R=2.20$ fm and $a=0.43$ fm, and was fitted. This potential is fixed in strength, with the fitted parameters $\mathrm{Re}b_0=0.25$ fm^3, $\mathrm{Im}b_0=-0.35$ fm^3, $\mathrm{Re}b_1=6.86$ fm^3, and $\mathrm{Im}b_1=6.16$ fm^3. These potentials will be referred to as $V_{\pi 1}$ and $V_{\pi 2}$, respectively.

As stated above the spin-dependent two-body *t*-matrix amplitudes were assumed to be the on-shell

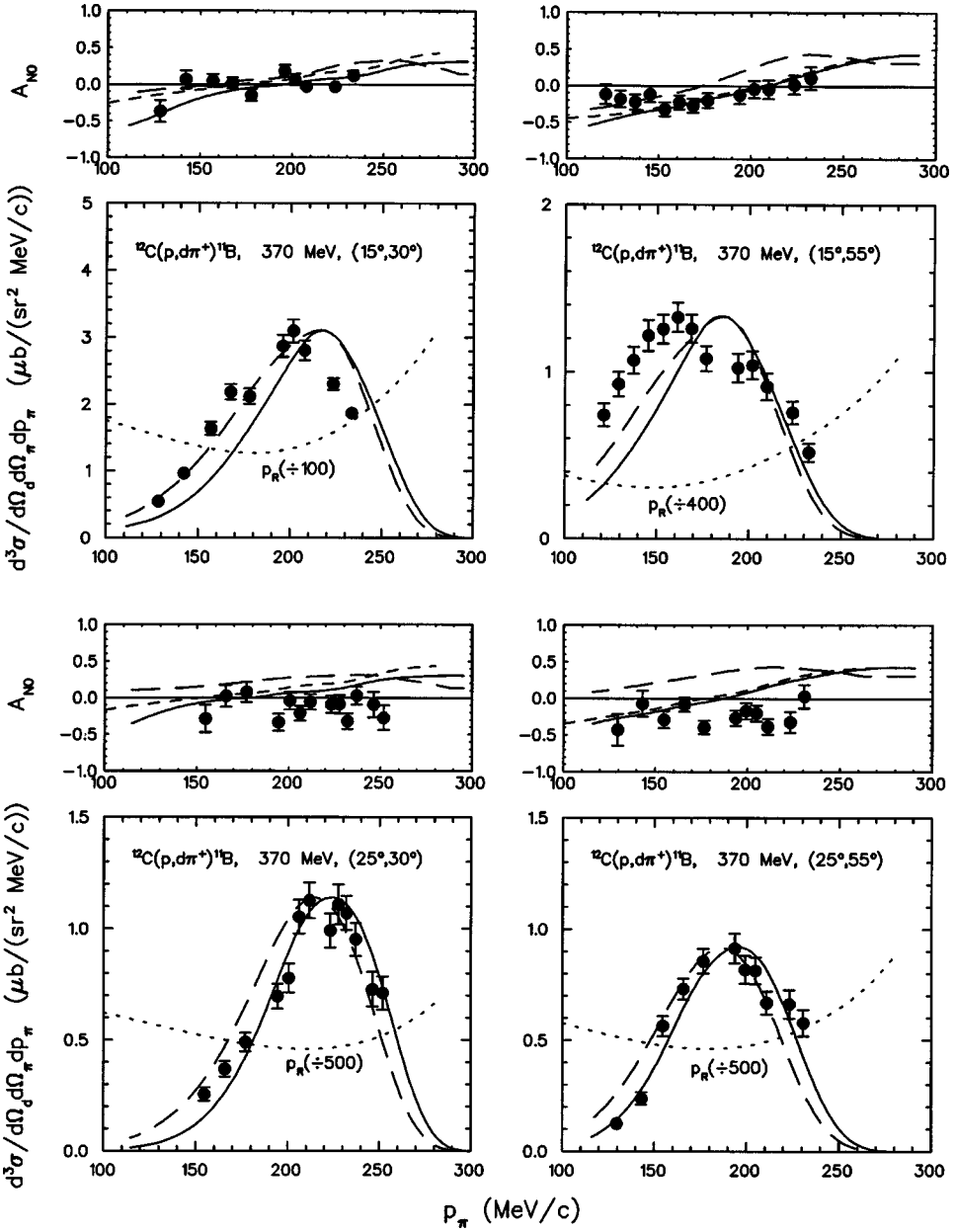

FIG. 10. The same as Fig. 9, with PWIA calculations RC3 (solid line), RC4 (long dashes), FC1 (short dashes, analyzing powers, only), as described in Table VI.

$pp \rightarrow d\pi^+$ amplitudes and were obtained from the phenomenological parametrization of Bugg, Hasan, and Shypit [16]. These amplitudes reproduce rather well the observed analyzing powers for the $\vec{p}p \rightarrow d\pi^+$ reaction, as well as the analyzing powers for the inverse $^2\mathrm{H}(\pi^+, pp)$ reaction, particularly at energies near the Δ resonance. Even with this on-shell assumption there are ambiguities in the choice of on-shell points to use in the calculations. Various prescriptions have been used, and in this work we have chosen the two most common, the initial energy prescription (IEP) and the final energy prescription (FEP). These correspond, respectively, to using the relative energy of the incident $p+p$ system, or using the final $d+\pi$ system, to evaluate the center-of-mass energies and angles for the two-body $pp \rightarrow d\pi^+$ system and thus the amplitudes. These prescriptions represent two rather extreme assumptions and, as such, they encompass the range of plausible off-shell effects that might be expected. For the conditions of this experiment the calculated two-body c.m. angle changes slowly across the energy sharing distribution, varying at most by 10° for any of the four angle pairs. (Note that the angle is the same for both on-shell prescriptions.) On the other hand the calculated two-body energy shows a significant variation of almost 30% across the energy sharing distributions. Thus much of the variation in the DWIA analyzing power arises from the energy dependence of the $\vec{p}p \rightarrow d\pi^+$ reaction. Using the above input parameters, DWIA as well as PWIA calculations were performed with the code THREEDEE [22] for both prescriptions.

PWIA calculations, quite independent of the ones discussed above, were also made that used the parametrization of the $pp \rightarrow d\pi^+$ reaction amplitudes employed by Falk [8]. Here the ^{12}C single particle states were very simply approxi-

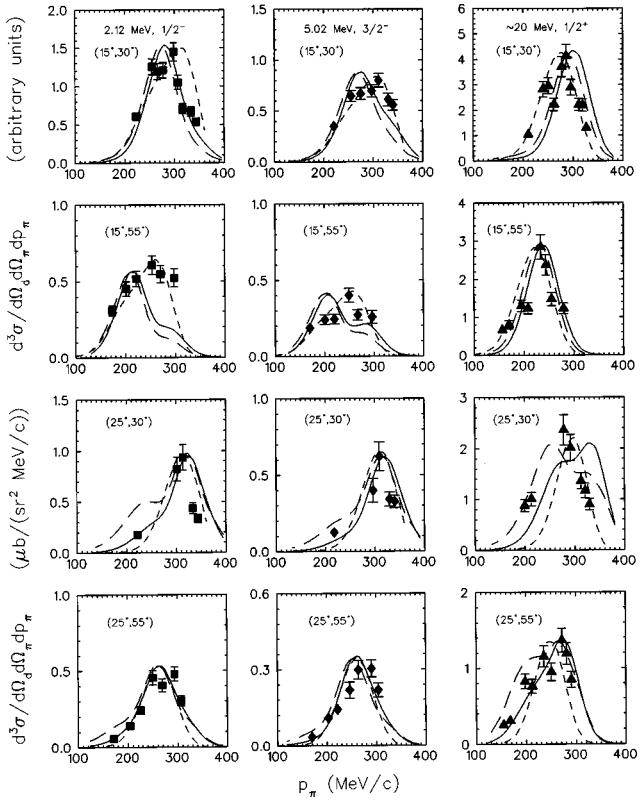

FIG. 11. Differential cross sections for $^{12}C(\vec{p},d\pi^+)^{11}B$ at 500 MeV for the excited states 2.12 MeV $1/2^-$ (left column), 5.02 MeV $3/2^-$ (center column), and $\approx$20 MeV excitation $1/2^+$ (right column). The curves are DWIA calculations RC7, RC9, and RC11 for the three states, respectively (solid line); RC8, RC10, and RC12 for the three states, respectively (long dashes); and PWIA calculations FC2, FC3, and FC4 for the three states, respectively (short dashes), as described in Table V. All quantities are expressed in the laboratory frame. The cross section curves have been normalized to the data as shown. For the 20 MeV state the cross sections represents a lower limit only.

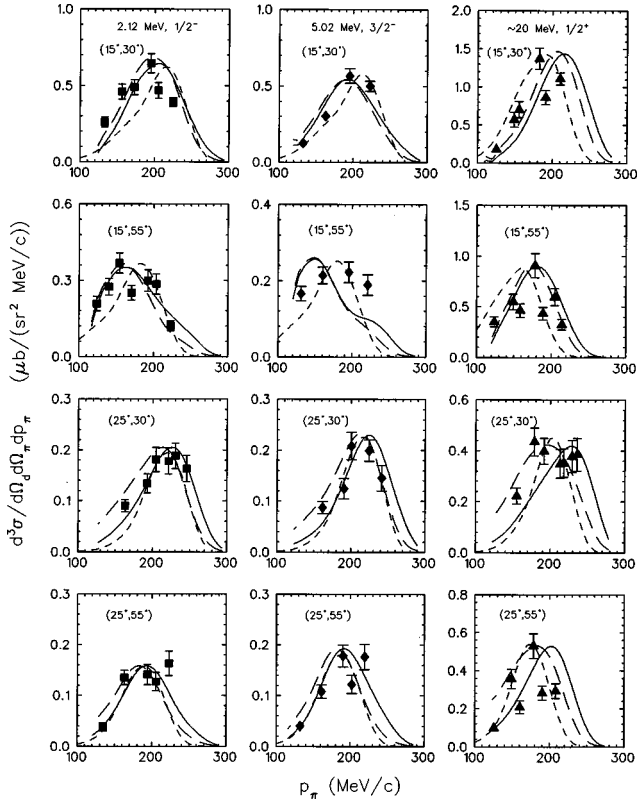

FIG. 12. Differential cross sections for $^{12}C(\vec{p},d\pi^+)^{11}B$ at 370 MeV for the excited states 2.12 MeV $1/2^-$ (left column), 5.02 MeV $3/2^-$ (center column), and $\approx$20 MeV excitation $1/2^+$ (right column). The curves are DWIA calculations RC5, RC7, and RC9 for the three states, respectively (solid line); RC6, RC8, and RC10 for the three states, respectively (long dashes); and PWIA calculations FC2, FC3 and FC4 for the three states, respectively (short dashes), as described in Table VI. All quantities are expressed in the laboratory frame. The cross section curves have been normalized to the data as shown. For the 20 MeV state the cross sections represents a lower limit only.

mated as harmonic oscillator (HO) functions using the HO parameter $\nu = 0.311$ fm^{-2}. Interestingly, the g.s. cross section distributions for such a simple ^{12}C wave function differed very little from those of the more detailed model. Results from these latter calculations will be shown for the analyzing powers and for the PWIA cross section distributions to excited states. These calculations thus provide an additional point of comparison of the parametrization of the $pp \rightarrow d\pi^+$ reaction amplitudes; they will be designated with the prefix *F*; those of the earlier discussion, by the prefix *R*.

B. Comparison with experiment

The angular acceptances of the spectrometers are quite large, as indicated by the information in Table II. Consequently, initial calculations were made to investigate the effects of the finite solid angles on the shapes and magnitudes of the differential cross sections. These investigations revealed that, for both ^2H and ^{12}C targets, the finite solid angle cross section predictions were smaller by 1 to 4 %, than the point solid angle predictions. Differences in shape were barely distinguishable on the graphs. Given the simplicity of the latter calculations, and also the fact that the overall normalization uncertainty was considerably greater than the above differences, all subsequent calculations and comparisons were made by using point solid angles, only.

1. The $^2H(\vec{p},d\pi^+)n$ reaction

PWIA calculations for the $^2H(\vec{p},d\pi^+)n$ reaction are shown in Fig. 6; they have been normalized to the data as shown. These calculated cross section distributions all tend to have rather narrow widths of approximately 50 MeV/*c* (FWHM). These widths are determined primarily by the slope of the momentum wave function in the region of 100 MeV/*c*. For the angle combination (15°,30°) at 500 MeV, the only case for which a fairly complete distribution was obtained, the experimental and calculated widths are in reasonable agreement, although there is a slight shift in momentum of the centroids of the distributions. The differences between the FEP and IEP calculations labeled RH1 and RH2, respectively, are not large, as expected, since the binding energy and the recoil energy carried off by the neutron are both small. However, they do lead to slight differences in the predictions for the analyzing powers, which describe reasonably well the experimental results.

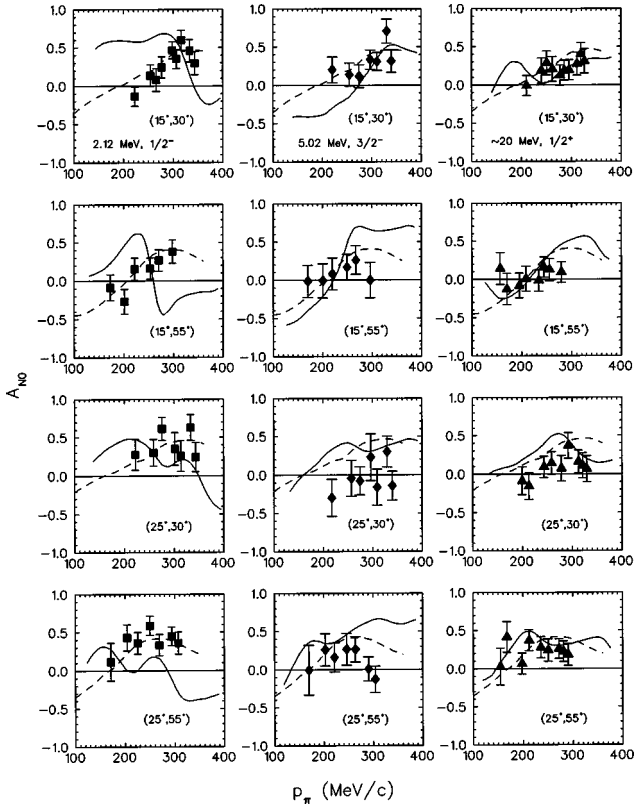

FIG. 13. Analyzing powers for the $^{12}C(\vec{p},d\pi^+)^{11}B$ at 500 MeV for the excited states 2.12 MeV $1/2^-$ (left column), 5.02 MeV $3/2^-$ (center column), and $\approx$ 20 MeV excitation $1/2^+$ (right column). The curves are DWIA calculations RC7, RC9, and RC11 for the three states, respectively (solid line); PWIA calculations FC2, FC3, and FC4 for the three states, respectively (short dashes), as described in Table V. All quantities are expressed in the laboratory frame.

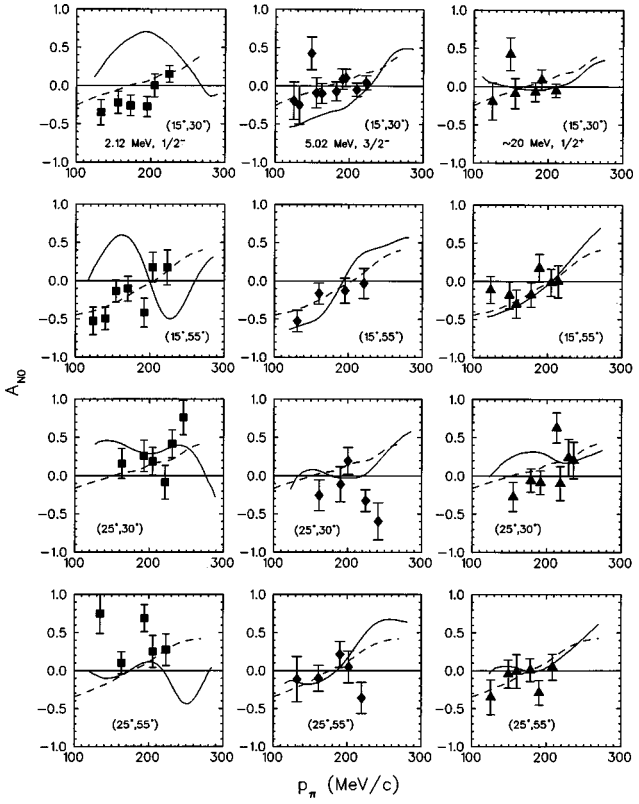

FIG. 14. Analyzing powers for the $^{12}C(\vec{p},d\pi^+)^{11}B$ at 370 MeV for the excited states 2.12 MeV $1/2^-$ (left column), 5.02 MeV $3/2^-$ (center column), and $\approx$ 20 MeV excitation $1/2^+$ (right column). The curves are DWIA calculations RC5, RC7, and RC9 for the three states, respectively (solid line); PWIA calculations FC2, FC3, and FC4 for the three states, respectively (short dashes), as described in Table VI. All quantities are expressed in the laboratory frame.

The extracted normalization factors (spectroscopic factors) $C^2S=\sigma_{\rm exp}/\sigma_{\rm theory}$ are shown in Table IV for the 370 MeV data; they have values of the order of unity. For reasons that remain unexplained, as indicated in Sec. III, instrumental difficulties rendered the 500 MeV cross section normalizations uncertain during the early part of the experiment.

2. The $^{12}C(\vec{p},d\pi^+)^{11}B$ g.s. reaction

Results for a number of calculations for the g.s. $^{12}C(\vec{p},d\pi^+)^{11}B$ reaction at 500 MeV are shown in Fig. 7. These DWIA calculations were intended to check the sensitivity of the predictions to various input assumptions. A summary of these and other calculations is given in Table V. Curves RC1 and RC2 compare calculations using the approximations FEP and IEP, respectively. The former invariably results in a cross section distribution that is shifted to a slightly higher pion momentum. Curves RC2 and RC3 compare calculations for the different deuteron potentials, described in Table III. All other parameters were kept the same. Finally, curves RC2 and RC4 compare calculations for different pion potentials, with all other parameters held constant. Figure 7 reveals that these substantial variations in the

TABLE III. Deuteron optical potentials.

		Nadasen adiabatic V_{d1}	Bojowald V_{d2}
Real potential	V_0 (MeV)	62.8	36.5
	r_0 (fm)	1.21	1.18
	a (fm)	0.77	0.714
Imag potential	W_0 (MeV)	14.8	20.46
	r_0' (fm)	1.688	1.27
	a' (fm)	0.44	0.815
Coulomb radius	r_C (fm)	1.25	1.30

TABLE IV. Spectroscopic factors C^2S for the $^2H(\vec{p},d\pi^+)n$ reaction.

	Calc.	DWIA	PWIA	IEP	FEP	Angle combination (15°,30°)	(15°,55°)
500 MeV	RH1		●		●		
	RH2		●	●			
	FH1		●		●		
370 MeV	RH1		●		●	1.47	0.94
	RH2		●	●		1.07	0.70
	FH1		●		●		

TABLE V. Spectroscopic factors C^2S for the $^{12}C(\vec{p},d\pi^+)^{11}B$ reaction at 500 MeV.

State	Calc. [a]	DWIA	PWIA	IEP	FEP	Angle combination (25°,30°)	Angle combination (25°,55°)
0.00 MeV, $3/2^-$	RC1	●			●	5.5	4.3
	RC2	●		●		8.1	6.1
	RC3 [b]	●		●		9.9	7.9
	RC4 [c]	●		●		7.3	5.9
	RC5		●		●	0.62	0.71
	RC6		●	●		0.84	1.00
	FC1		●		●		
2.12 MeV, $1/2^-$	RC7	●			●	2.00	2.40
	RC8	●		●		3.00	3.30
	FC2		●		●		
5.02 MeV, $3/2^-$	RC9	●			●	0.94	1.02
	RC10	●		●		1.46	1.46
	FC3		●		●		
$\approx$ 20 MeV, $1/2^+$	RC11	●			●	11.0	13.0
	RC12	●		●		15.6	22.6
	FC4		●		●		

[a]Standard potentials, including V_{d1} and $V_{\pi 1}$, were used for all calculations as described in the text, except where noted.
[b]Deuteron potential V_{d2}.
[c]Pion potential $V_{\pi 2}$.

potential parameters, or changes in the assumptions (FEP or IEP) made, result in comparatively small changes in the predicted cross section distributions. Indeed, these variations are considerably smaller than the differences between the data and the predictions. The lack of sensitivity to the potential parameters, especially the pion potential, is quite surprising. At a pion momentum of 260 MeV/c the pion mean free path in nuclear matter is at a minimum and changes rapidly as the pion momentum is either increased or decreased from this value.

Particularly striking is the discrepancy between the DWIA calculations and the data for the angle combination (15°,55°). Only at this angle combination does the cross section data show a much broader distribution, quite unlike the typically Gaussian distributions at the other angles. This same feature is repeated again in the 370 MeV data (see Fig. 9). The p-shell momentum wave function of ^{12}C has a broad maximum at a momentum of $\approx$120 MeV/c. Since $\approx$120 MeV/c is also the region of recoil nucleus momentum sampled by these measurements at $\theta_d = 15°$, this peculiar result at $\theta_\pi = 55°$, may arise from some complicated interplay of structure and medium effects. At the other extreme, for the angle combination (25°,55°), cross section data and DWIA calculations tend to agree best, revealing a symmetric and narrow peak. At $\theta_d = 25°$, the sampled recoil momentum is in the neighborhood of $\approx$200 MeV/c; here the single particle momentum wave function is well into the asymptotic region, with a well defined slope. This slope appears to be the defining characteristic reflected in the cross section distribution.

An examination of the spectroscopic factors C^2S as given in Table V for these calculations, shows some surprises. For the angle combinations with $\theta_d = 25°$, $S \approx 7$. From other experiments, to be discussed later [18], one expects a value of about 3. For reasons mentioned earlier in connection with the $^2H(\vec{p},d\pi^+)n$ reaction, reliable spectroscopic factors were not obtained for the first two angle combinations with $\theta_d = 15°$.

The analyzing power predictions shown in Fig. 7 display the general trend of the data at low recoil nucleus momentum ($\theta_d = 15°$), but do not agree quantitatively. At high recoil nucleus momentum ($\theta_d = 25°$) all the calculations disagree with the data.

A series of PWIA calculations were also made for the 500 MeV $^{12}C(\vec{p},d\pi^+)^{11}B$ reaction. These are shown in Fig. 8. For the cross sections, other than the expected large change in magnitude, the most notable difference from the DWIA results is the substantial shift to higher pion momentum of the peak of the distributions for the low recoil momentum angles, a shift that produces better agreement with the data. On the other hand, the PWIA predictions at the high recoil momentum angles differ little from the DWIA predictions. However, the most surprising result is the observation that the analyzing powers are better described by the PWIA results; indeed, for low recoil momentum they represent a good fit to the data. This is most unexpected since we expected the effective polarization to be large and thus anticipated that the spin-correlation parameter A_{00nn} would have a major effect on the beam analyzing powers. Comparisons of

TABLE VI. Spectroscopic factors C^2S for the $^{12}C(\vec{p},d\pi^+)^{11}B$ reaction at 370 MeV.

State	Calc. [a]	DWIA	PWIA	IEP	FEP	Angle Combination (15°,30°)	(15°,55°)	(25°,30°)	(25°,55°)
0.00 MeV, $3/2^-$	RC1	●			●	4.60	4.43	3.34	4.36
	RC2	●		●		3.07	3.02	2.44	3.11
	RC3		●		●	0.41	0.45	0.51	1.00
	RC4		●	●		0.30	0.33	0.36	0.73
	FC1		●		●				
2.12 MeV, $1/2^-$	RC5	●			●	1.27	2.21	0.88	1.17
	RC6	●		●		0.77	1.23	0.57	0.83
	FC2		●		●				
5.02 MeV, $3/2^-$	RC7	●			●	1.13	1.20	0.82	1.10
	RC8	●		●		0.68	0.75	0.58	0.75
	FC3		●		●				
$\approx$ 20 MeV, $1/2^+$	RC9	●			●	5.0	4.0	3.0	5.2
	RC10	●		●		2.9	2.3	2.0	4.2
	FC4		●		●				

[a]Standard potentials, including V_{d1} and $V_{\pi 1}$, were used for all calculations as described in the text.

the DWIA and PWIA results clearly show that this is borne out by the calculations. However, the data do not reflect this, agreeing better with the PWIA calculations.

The absolute spectroscopic factors extracted from PWIA calculations are not expected to be meaningful for the $^{12}C(\vec{p},d\pi^+)^{11}B$ reaction. Nevertheless, the relative spectroscopic factors may provide helpful insights; they tend to be fairly consistently smaller by about a factor of 8 than the ones obtained from the DWIA calculations. These are shown in Table V, as well.

Calculations intermediate between the DWIA and PWIA ones described above, where, in turn, plane waves for the proton, deuteron and pion, were used, were also explored. These predictions fell smoothly between those previously described and revealed no particular sensitivities to any one of the proton, deuteron or pion waves.

Figures 9 and 10 present DWIA and PWIA calculations, respectively, for the $^{12}C(\vec{p},d\pi^+)^{11}B$ g.s. reaction at 370 MeV. Many of the qualtitative features of these predictions are similar to those for 500 MeV. The shift in the peak of the cross section distributions to higher momentum for the PWIA results, relative to the DWIA results, is again observed for $\theta_d = 15°$. The DWIA calculations reproduce the shapes of the cross section data rather well, except at the angle combination (15°,55°). The PWIA results also describe the shapes of the cross section data well at the higher recoil momentum ($\theta_d = 25°$). Spectroscopic factors for the 370 MeV results are shown in Table VI. These numbers are relatively constant as a function of angle and, for the DWIA case, have values of about 4 and 3 for the FEP and IEP calculations, respectively.

The analyzing powers for the g.s. $^{12}C(\vec{p},d\pi^+)^{11}B$ reaction at 370 MeV are also shown in Figs. 9 and 10. Again, as at 500 MeV, the DWIA calculations do not fit the data; also, as before, the PWIA calculations, especially calculations RC3 and FC1, fit the low recoil momentum cases very well.

3. The $^{12}C(\vec{p},d\pi^+)^{11}B$ reaction to excited states

Cross section data for excited states at 500 and 370 MeV are shown in Figs. 11 and 12, respectively. In these figures the four angle pairs for each of the states 2.12 MeV $1/2^-$, 5.02 MeV $3/2^-$, and $\approx$20 MeV $1/2^+$ are arranged in vertical columns. The continuum, resulting from the interaction of the incoming proton with a *s*-shell proton, has a broad distribution, as discussed in connection with Fig. 5. This distribution had a peak at $\approx$20 MeV excitation, although, it must be stressed, only part of this continuum was measured in this experiment. Acceptance of the spectrometers was such that measurements at additional spectrometer settings would have been required to map out this continuum completely. Hence, the cross sections represented in these plots for $\approx$20 MeV excitation are a lower limit only, and furthermore, a variable fraction of this cross section. While as much as 80% of the cross section may have been measured near the peak of the cross section distribution, considerably less than this was measured in the tails of the distribution. Nevertheless, these cross sections are at least 50% as large as those for the g.s. As expected for *p*-shell removal, the shapes of the cross section distributions for the 2.12 and 5.02 MeV states are very similar to those for the g.s., with comparable widths and peak locations defined by the minimum in the recoil momentum. Their strengths are considerably smaller than for the g.s., in keeping with the results observed in the $^{12}C(d,^3He)^{11}B$ reaction [18].

Results for DWIA and PWIA calculations for the excited states are also shown in Figs. 11 and 12. No detailed structure was assumed for these states; they were simply represented by single-particle wave functions calculated in a

Woods-Saxon potential. The DWIA predictions for the FEP and IEP calculations are very similar at low recoil momentum for each of the 2.12 and 5.02 MeV states. At the higher recoil momenta, and for increasing excitation, the locations of the peaks are separated by increasing amounts. The experimental cross section distributions tend to be broader at the angle pair (15°,55°) than the DWIA predictions. On the other hand, the PWIA predictions reproduce the observations quite well. Spectroscopic factors extracted from these plots are given in Tables V and VI; they will be discussed in Sec. VI.

Especially interesting are the analyzing power data and calculations for excited states at 500 and 370 MeV shown in Figs. 13 and 14, respectively. Here only the FEP DWIA results are shown; the IEP DWIA predictions are rather similar. In the DWIA calculations presented in the figures, one clearly observes the contributions of the effective nucleon polarization. This is especially clear from a comparison of the $p_{1/2}$ (2.12 MeV) and the $p_{3/2}$ (5.02 MeV) states for which the contribution of the effective polarization is of opposite sign. This contribution clearly indicates that the DWIA calculated effective polarization is large, and it leads to considerable structure and/or large variations in the analyzing powers as a function of pion momentum. As for the ground state, the DWIA calculations are in poor agreement with the data. The FEP PWIA predictions, on the other hand, represent the data rather well, in most cases. Although the statistics are relatively poor, the analyzing power data for all three states (the *p* states with an effective polarization contribution and the *s* state with none) are quite similar. This suggests that the DWIA grossly overpredicts the effective polarization, a rather surprising outcome for the strongly absorbed particles.

VI. DISCUSSION AND CONCLUSIONS

The initial surprise at the insensitivity of the DWIA calculations to the input optical potentials prompted further investigations by using an inner radial cutoff. For an inner radial cutoff of 2.5 fm (just inside the nuclear surface of $\approx$2.8 fm) the DWIA cross sections were reduced by $\approx$20 and $\approx$30 %, respectively, for $\theta_d = 15°$ and $\theta_d = 25°$. The Fourier transform of a *p*-shell Woods-Saxon wave function is reduced in amplitude to 81 and 52 % at momenta of 100 and 200 MeV/*c*, respectively, for the above cutoff, relative to the case with no cutoff. Allowing for the role of some distortions, the observed reductions in the cross sections are not unreasonable. Hence, the $(p,d\pi^+)$ reaction at these relatively modest recoil momenta is strongly surface localized.

Spectroscopic factors for proton pickup from ^{12}C have previously been investigated with the $^{12}C(d,^3He)^{11}B$ reaction [18]. For the states of interest in the present experiment, the g.s. $3/2^-$, the 2.12 MeV $1/2^-$, and 5.02 MeV $3/2^-$ states, the extracted values of C^2S are 2.98, 0.69, and 0.31, respectively, from proton pickup. As noted in the earlier discussion, and presented in Tables V and VI, the values of C^2S extracted from the present $^{12}C(\vec{p},d\pi^+)^{11}B$ reaction and DWIA calculations are not constant, but vary by factors of 2–3 from the above values. The absolute values of C^2S at 500 MeV are significantly too large, possibly suggesting an overattenuation due to the distorting potentials. This interpretation is supported by the value of the extracted spectroscopic factor for the $s_{1/2}$ shell, which is about twice as large as for the g.s.; one expects a value about 2/3 as large. Since the $s_{1/2}$ shell wave function is more strongly concentrated in the nuclear interior, this overattenuation would lead to underprediction of the cross section. At 370 MeV the $s_{1/2}$ spectroscopic factor is comparable to that for the g.s. Here the relative strengths of the spectroscopic factors, as well as their absolute values are in much better agreement, suggesting that the attenuation problem is less severe at this energy. Nevertheless, the variations observed, which are a function of recoil momentum and bombarding energy, indicate that the dynamics of the reaction are not adequately described within the present model. On the other hand, the considerable level of agreement attained does suggest that the assumption that the $^{12}C(\vec{p},d\pi^+)^{11}B$ reaction is mediated by the two-body $pp \rightarrow d\pi^+$ reaction is qualitatively correct.

The most surprising result from the comparison of the DWIA calculations with the data is the fact that the analyzing powers are generally poorly described. The PWIA calculations (with FEP), on the other hand, describe the analyzing powers rather well for the low recoil momentum cases. The effective nucleon polarization predicted by the DWIA calculations for the g.s. (calculated assuming the spin-orbit potential of the incident proton could be ignored) is very large, reaching values approaching unity. Furthermore, it is characterized by a rather sharp transition from positive to negative polarization as the pion momentum is increased. This is in marked contrast to the free nucleon picture of the PWIA calculations (no effective polarization), which reproduce the analyzing powers reasonably well, as noted. Experimentally, there is little distinction in the shapes of the analyzing power distributions among the different states, including the $s_{1/2}$ hole state. At the higher recoil momenta there is some suggestion that the analyzing powers for the 2.12 MeV $1/2^-$ state are more positive than for the $3/2^-$ states. However, because of the large statistical errors, it is difficult to draw firm conclusions. The effective nucleon polarization in $p_{1/2}$ and $p_{3/2}$ states from distortion effects is clearly seen in $(p,2p)$ reactions, leading to analyzing powers of opposite sign [32] as, for example, in ^{16}O. The present DWIA calculations for the $^{12}C(\vec{p},d\pi^+)^{11}B$ reaction do, indeed, show such effective polarization, as can be seen by comparing the predictions for the analyzing powers for the 2.12 and 5.02 states at the same angles in Fig. 13. The experimental observations are not in accord with these predictions, once again suggesting that there are difficulties associated with the treatment of the distortions. Thus the problems related to both the spectroscopic factors and the analyzing powers may be attributable to a deficiency in the optical model treatment of this aspect of the reaction mechanism. To further investigate this effect high statistics measurements on the $^{16}O(\vec{p},d\pi^+)^{15}N$ reaction would be most helpful, where the ^{16}O target has nominally filled $p_{1/2}$ and $p_{3/2}$ shells.

In the present study we have shown that many features of the $^{12}C(\vec{p},d\pi^+)^{11}B$ reaction can be understood, assuming that the pion production mechanism is mediated by the $pp \rightarrow d\pi^+$ process. The shapes of the cross section distributions, with few exceptions, are reproduced by the DWIA and PWIA calculations, although the extracted spectroscopic factors are not constant. Where the DWIA and PWIA predic-

tions differ markedly is for the analyzing powers; here also further studies are required to explore this behavior. Because of the general level of success of the model, we have tended to attribute many of the difficulties to inadequate optical model potentials for the various distorted waves. There is, however, another aspect which potentially could be a source of difficulty. In particular, at the present energies the formation of a Δ dominates the two-body process. It is possible that the propagation of the Δ in the medium causes the reaction to be much less localized, whereas the DWIA assumes a localized interaction. In that case perhaps the effective polarization which is associated with this localization is not a good concept. In addition there may be strong spin-dependent effects in the Δ-nucleus interaction which can modify the spin observables. Such an effect has been suggested in studies of $^7\mathrm{Li}(\pi^+,\pi^+p)^6\mathrm{He}$ on a polarized target [33]. To sort out the various possibilities additional data are needed, particularly data for spin-orbit partners, and also at several energies, so that the role of the Δ might be better understood.

When these issues are better understood fruitful extensions of the experimental investigations to higher recoil momenta should be undertaken. Results from such investigations would have important implications for understanding nuclear pion production in two-body $^ZA(\vec{p},\pi^+)^Z(A+1)$ reactions [8]. Also important to this understanding is the present observation of the large strength to the $s_{1/2}$ state in the $^{12}\mathrm{C}(\vec{p},d\pi^+)^{11}\mathrm{B}$ reaction. Many final states in the $^Z\mathrm{A}(\vec{p},\pi^+)^Z(A+1)$ reaction can be reached via interactions of the incoming proton with protons from all the various shells. Such contributions can interfere, giving rise to the complex structure that is observed in the angular distributions of the differerential cross sections and the analyzing powers.

ACKNOWLEDGMENTS

This work was supported in part by the Natural Sciences and Engineering Research Council of Canada. Useful discussions with N.S. Chant are gratefully acknowledged.

[1] E. G. Auld, A. Haynes, R. R. Johnson, G. Jones, T. Masterson, E. L. Mathie, D. Ottewell, P. Walden, and B. Tatischeff, Phys. Rev. Lett. **41**, 462 (1978).
[2] T. P. Sjoreen, P. H. Pile, R. E. Pollock, W. W. Jacobs, H. O. Meyer, R. D. Bent, M. C. Green, and F. Soga, Phys. Rev. C **24**, 1135 (1981).
[3] E. Korkmaz, S. E. Vigdor, W. W. Jacobs, T. G. Throwe, L. C. Bland, M. C. Green, P. L. Jolivette, and J. D. Brown, Phys. Rev. C **40**, 813 (1989); E. J. Korkmaz, Ph.D. thesis, Indiana University, 1987, and references therein.
[4] E. Korkmaz, L. C. Bland, W. W. Jacobs, T. G. Throwe, S. E. Vigdor, M. C. Green, P. L. Jolivette, and J. D. Brown, Phys. Rev. Lett. **58**, 104 (1987).
[5] G. M. Huber, G. J. Lolos, E. L. Mathie, Z. Papandreou, K. H. Hicks, P. L. Walden, S. Yen, X. Aslanoglou, E. G. Auld, and W. R. Falk, Phys. Rev. C **36**, 1058 (1987).
[6] G. M. Huber, G. J. Lolos, R. D. Bent, K. H. Hicks, P. L. Walden, S. Yen, X. Aslanoglou, E. G. Auld, and W. R. Falk, Phys. Rev. C **37**, 1161 (1988).
[7] W. R. Falk, E. G. Auld, G. Giles, G. Jones, G. J. Lolos, W. Ziegler, and P. L. Walden, Phys. Rev. C **33**, 988 (1986).
[8] W. R. Falk, Phys. Rev. C **50**, 1574 (1994).
[9] A. A. Cowley, P. G. Roos, J. J. Lawrie, F. D. Smit, J. V. Pilcher, S. V. Förtsch, G. F. Steyn, and G. C. Hillhouse, Phys. Rev. C **45**, 1745 (1992).
[10] R. Abegg, W. P. Alford, D. Frekers, K. Hicks, R. Schubank, P. Walden, and S. Yen, TRIUMF internal report, 1985.
[11] M. Vetterli *et al.*, TRIUMF internal report, 1990.
[12] K. H. Hicks, TRIUMF internal report, 1988.
[13] S. Yen, TRIUMF design note, Report No. TRI-DN-88-10, 1988.
[14] P. Walden *et al.* (unpublished).
[15] G.L. Giles, Ph.D. thesis, University of British Columbia, 1985.
[16] D. V. Bugg, A. Hasan, and R. L. Shypit, Nucl. Phys. **A477**, 546 (1988); D. V. Bugg *ibid.* **A437**, 534 (1985).
[17] P. W. Green, TRIUMF Report No. TRI-DNA-91-1, 1991.
[18] G. Mairle and G. J. Wagner, Nucl. Phys. **A253**, 253 (1975).
[19] K. L. Brown, F. Rothacker, D. C. Carey, and Ch. Iselin, Report No. SLAC-91, 1977.
[20] N. S. Chant and P. G. Roos, Phys. Rev. C **15**, 57 (1977).
[21] N. S. Chant and P. G. Roos, Phys. Rev. C **27**, 1060 (1983).
[22] N. S. Chant, computer code THREEDEE, University of Maryland (unpublished).
[23] P. G. Roos and N. S. Chant, Phys. Rev. C **52**, 2591 (1995).
[24] N. S. Chant and P. G. Roos, Phys. Rev. C **38**, 787 (1988).
[25] H. C. Newns, Proc. Phys. Soc. London, Sect. A **66**, 477 (1953); H. C. Newns and M. Y. Refai, *ibid.* **71**, 627 (1958).
[26] G. Jacob, Th.A.J. Maris, C. Schneider, and N. R. Teodoro, Nucl. Phys. **A257**, 517 (1976).
[27] L. R. B. Elton and A. Swift, Nucl. Phys. **A94**, 52 (1967).
[28] E. D. Cooper, S. Hama, B. C. Clark, and R. L. Mercer, Phys. Rev. C **47**, 297 (1993).
[29] A. Nadasen *et al.* Phys. Rev. C **23**, 1023 (1981).
[30] J. Bojowald *et al.* Phys. Rev. C **38**, 1153 (1988).
[31] W. B. Cottingame and D. B. Holtkamp, Phys. Rev. Lett. **45**, 1828 (1980).
[32] P. Kitching, W. J. McDonald, Th.A.J. Maris, and C. A. Z. Vasconcellos, Adv. Nucl. Phys. **15**, 43 (1985).
[33] M. G. Khayat, Ph.D. thesis, University of Maryland, 1995.